Ultrastructural analysis reveals mitochondrial placement independent of synapse placement in fine caliber C. elegans neurons.

Danielle V. Riboul,[1] Sarah Crill,[2] Carlos Oliva,[2] Maria Gabriela Restifo,[2] Reggie Joseph,[2] Kerdes Joseph,[3] Ken C.Q. Nguyen,[4] David H. Hall,[4] Yaouen Fily[2] and Gregory T. Macleod,[2,5,6,7]*

1. Integrative Biology & Neuroscience Graduate Program, Florida Atlantic University, Boca Raton, FL 33431, USA
2. Wilkes Honors College, Florida Atlantic University, Jupiter, FL, 33458, USA
3. Department of Biology, C.E.S. College of Science, Florida Atlantic University, Boca Raton, FL, 33431, USA
4. Department of Neuroscience, Albert Einstein College of Medicine, Bronx, NY 10461, USA.
5. Jupiter Life Sciences Initiative, Florida Atlantic University, Jupiter, FL 33458, USA
6. Brain Institute, Florida Atlantic University, Jupiter, FL 33458, USA
7. Institute for Human Health & Disease Intervention (I-HEALTH), Florida Atlantic University, Jupiter, FL 33458, USA
* Correspondence: macleodg@fau.edu

Abbreviated Title: Neuronal control of mitochondria in *C. elegans*

Keywords: mitochondria, synapses, electron microscopy

Number of Text Pages: 28
Number of Figures: 6 main figures, 2 supplemental figures, 8 supplemental tables
Number of Words: Summary 229, Significance 120, Introduction 584, Results 1763, Discussion 871

Conflict of Interest Statement: The authors declare no competing financial interests.

Acknowledgements: This work was supported by NIH NINDS awards NS103906 and NS123377 to GTM and NIH R24 OD010943 to DHH. We are grateful for discussions with Drs Guy Benian and Ivanov Stoyan. We thank John White and Jonathan Hodgkin for sending the collected TEM images of the MRC/LMB lab of Sydney Brenner to the Hall lab for long term conservation and sharing on WormImage (also supported by NIH R24 OD010943).

SUMMARY:

Neurons rely on mitochondria for an efficient supply of ATP and other metabolites. However, while neurons are highly elongated, mitochondria are discrete and limited in number. Due to the slow rates of diffusion of long distances it follows that neurons would benefit from an ability to control the distribution of mitochondria to sites of high metabolic activity, such as synapses. It is assumed that neurons' possess this capacity, but ultrastructural data over substantial portions of a neuron's extent that would allow for tests of such hypotheses are scarce. Here, we mined the *Caenorhabditis elegans'* electron micrographs of John White and Sydney Brenner and found systematic differences in average mitochondrial size (ranging from 1.4 to 2.6 μm), volume density (3.8% to 7.1%) and diameter (0.19 to 0.25 μm) between neurons of different neurotransmitter type and function, but found no differences in mitochondrial morphometrics between axons and dendrites of the same neurons. Analyses of distance intervals found mitochondria to be distributed randomly with respect to both presynaptic and postsynaptic specializations. Presynaptic specializations were primarily localized to varicosities, but mitochondria were no more likely to be found in synaptic varicosities than non-synaptic varicosities. Consistently, mitochondrial volume density was no greater in varicosities with synapses. Therefore, beyond the capacity to disperse mitochondria throughout their length, at least in *C. elegans*, fine caliber neurons manifest little in the way of subcellular control of mitochondria.

SIGNIFICANCE:

Brain function is unequivocally reliant on mitochondrial function for its energy needs, and the mechanisms that cells use to control these organelles is an active field of enquiry. WormImage, a decades old electron microscopy database in the public domain, contains information about the ultrastructural disposition of mitochondria within the nervous system over previously unexamined extents. In a largely remote format, a team of undergraduate students, coordinated by a graduate student, mined this database over the course of the pandemic. We found heterogeneity in mitochondrial size and density between, but not within, the fine caliber neurons of *C. elegans*. While neurons are clearly able to disperse mitochondria throughout their extent, we found little evidence that that they "install" mitochondria at synapses.

INTRODUCTION:

Neurons are highly elongated, allowing them to communicate over long distances, but their morphology presents challenges for small outposts with high metabolic demands, such as synapses. Mitochondria are essential components of neuronal metabolism, and, among other functions, they generate ATP, buffer Ca^{2+} and contribute to neurotransmitter synthesis at synapses (Devine and Kittler, 2018). However, due to the limitations to diffusion of both mitochondria and metabolites, neurons need mechanisms to move mitochondria to, and/or concentrate them, where they are most needed. Motor-based transport distributes mitochondria along microtubules and microfilaments to a neuron's furthest extent (Kruppa and Buss, 2021), while other mechanisms can arrest their movement or anchor them in place. For example, posttranslational modification of microtubules modifies motor-based transport (Hammond et al., 2010), local elevations in Ca^{2+} arrest mitochondrial movement through the agency of the adaptor protein *miro* (Wang and Schwarz, 2009), *syntaphilin* anchors mitochondria along axons (Kang et al., 2008), and membrane interactions arrest mitochondrial adjacent to other organelles (Lebiedzinska et al., 2009). This list is far from exhaustive, but it demonstrates numerous mechanisms available to modify motor-based dissemination of mitochondria, presumably to position them where they are most needed.

Our common understanding that neurons distribute mitochondria to synapses, and exert subcellular control of mitochondrial morphology and volume density, is based on fluorescence light microscopy data and electron microscopy data. However, limitations of both techniques leaves room for reinterpretation of the data. The spatial resolution of light microscopy is inadequate for the purposes of estimating mitochondrial number, morphology or volume density, especially when they are densely intertwined (Turner et al., 2022). Electron microscopy, while providing exceptional resolution, has a greatly limited field of view, which generally excludes the opportunity to sample neurons in their entirety, or to sample ultrastructural features in sufficient numbers for statistical analyses. There are notable exceptions. Super-resolution techniques have increased light microscopy resolution of mitochondria and synapses by an order of magnitude (Huang et al., 2008; Sigal et al., 2015), but the fields of view have shrunk commensurately. Automation of aspects of the electron microscopy work flow have allowed for the reconstruction of greater volumes of nervous tissues (yet still < 1% of 1 cubic millimeter) in both mammals and invertebrates (Turner et al., 2022; Winding et al., 2023), although these data repositories have yet to reveal the disposition of individual mitochondria relative to each other, or relative to synapses. Analysis likely trails the acquisition of the data because of the difficulty in automating and validating protocols to quantify distances and volumes between mitochondria and synapses within the organic shapes of neuronal processes.

In this study, analysis trails data acquisition by 40 years. We examined transmission electron micrographs spanning a 442 μm length of *C. elegans*, reconstructing motor neurons, interneurons and sensory neurons in the N2U series (White et al., 1986). The unambiguous identification of each neuron, high quality of mitochondrial profiles, recent revision of synapse annotation (Cook et al., 2019) and the relatively simple morphology of these neurons gave an unprecedented opportunity to interrogate the disposition of individual mitochondria relative to each other and to synapses. We observed differences in mitochondrial morphometrics between neuron types, but we found little evidence for either subcellular control of mitochondrial volume density or a mechanism that controlled mitochondrial approach to synapses. While neurons in *C. elegans* generally do not rely on classical all-or-none Na^+-based action potentials (Lockery and Goodman, 2009), these data never-the-less raise questions about whether we should anticipate a similar lack of mitochondrial control in fine caliber neurons in vertebrates *in vivo*.

RESULTS:

Neurons can be reconstructed in their entirety from WormImage electron micrographs

Transmission electron micrographs collected from the *C elegans* N2U section series allowed us to reconstruct neurons over a substantial extent of their length. We examined micrographs labeled #1 to 1763 on the dorsal side of the N2U series and #1 to 1844 on the ventral side (Fig. 1A). Sequentially labeled micrographs posterior to the esophageal ganglion represent every 3rd section of a larger series of sections cut at 80 nm intervals (Cook et al., 2019). Using ImageJ software we separately measured the cross-sectional areas of neuronal profiles, and the mitochondria contained within (Fig. 1A). Fifteen (15) neurons were selected to represent a manageable sample of the neurotransmitter and functional diversity, yet still providing repetition across 5 neuron types; GABAergic motor neurons (3), cholinergic motor neurons primarily innervating body wall muscles (3), cholinergic motor neurons primarily innervating vulval muscles (3), cholinergic interneurons (4) and glutamatergic sensory neurons (2) (Fig. 1B). Each neuron is represented in silhouette where its diameter was calculated from the area of the neuronal profile rendered as a perfect circle. The GABAergic motor neurons have both dorsal and ventral processes connected by commissures. The series covered between 28 and 100 % of the longitudinal extent of 15 neurons, (69 ± 28%; mean ± SD), capturing the somata of all 9 motor neurons (Fig. 1B).

The lateral extent of mitochondrial profiles can be reconstructed in 5 nm resolution

The N2U series was originally photographed at 45,000X magnification (White et al., 1986) and our measurements were made on scanned images of these micrographs digitized at 5 nanometers per

pixel (Fig. S1), providing ~ 5 nm resolution orthogonal to the long axis of the worm. Mitochondrial profiles could be resolved with strong contrast, often allowing discrimination of the outer membrane separate from the inner membrane and showing cristae structure (Fig. 2A-E, panels on left). Neurons in each micrograph are annotated with a handwritten identifying number (Fig.2A-E, panels on left), and the extent of each mitochondrion is represented within each neuron, centered on the long axis (Fig.2A-E, panels on right).

Mitochondrial diameter and density differ systematically between the five neuron types

Parameters of mitochondrial size and shape were analyzed in neuronal processes, i.e. all parts of the neuron excluding the cell body. Average mitochondrial length and volume were calculated for each of the 5 neuron types and mitochondria were found to be twice as large in cholinergic interneurons (length and volume; Fig. 2F-G). Average mitochondrial diameters have a tight variance and appear to be under exquisite control, with mitochondria in VC-type cholinergic motor neurons having the “thinnest” mitochondria (Fig. 2H). Average neuronal diameter is also tightly controlled, with command interneurons and GABAergic motor neurons having the largest calibers (Fig. 2I). A plot of mitochondrial diameter against mitochondrial length showed no association indicating that mechanisms determining length and diameter can work independently (Fig. S2A; $P = 0.85$). Mitochondrial diameter will necessarily be constrained by neuron diameter, and so mitochondrial diameter was plotted against neuron diameter to test for evidence consistent of a causal relationship. Here too, correlational analysis showed no association between the two, thus ruling out mitochondrial diameter as a simple function of neuron diameter (Fig. S2B; $P = 0.26$). Instantaneous mitochondrial density, i.e. that proportion of a neuron’s cross-sectional area occupied by a mitochondrion, was distinct in all 5 neuron types, with VB-type motor neurons having double the instantaneous density of interneurons, despite releasing a common neurotransmitter; acetylcholine (Fig. 2J). Finally, overall mitochondrial density calculations showed VC-type cholinergic motor neurons to have a density of only 3.8%, while the other 4 neuron types grouped in a range with almost twice the density (between 5.7% and 7.1%; Fig. 2K).

Little evidence for differential subcellular control of mitochondrial size and density

In an initial test of the neurons’ capacity for subcellular control of mitochondrial morphology and volume density we compared parameters measured in Figure 2F-K between different neuronal compartments. Each neuron might be divided into different compartments according to which portion is in the ventral versus dorsal nerve cord, which portions are cellular processes versus the cell body (soma), and which portions are primarily dendritic versus axonal. The latter distinction was made by annotating each neuron profile with the micrograph/section location of

either presynaptic (blue section) or postsynaptic specializations (pink section) while cross checking with add ref (Fig. 3A-C).

In a comparison between mitochondria in the “dendritic” portions of cholinergic motor neurons DD3, VD4 and VD5, and those in portions with both pre- and postsynaptic synaptic elements, mitochondrial diameter but not length registered as significantly different (diameter: P=0.005; length: P=0.496; N=3; Fig. 3D,E). Mitochondrial density was no different (P=0.999; Fig. 3F). In a comparison between mitochondria in dorsal versus ventral portions of the motor neurons, where ventral portions are also happen to be closest to the soma, no morphometric aspect registered as being significant (Fig. 3D-F). Finally, in a comparison between mitochondria in motor neuron processes versus those in the soma, we observed that mitochondrial diameter but not length registered as significantly different (diameter: P=0.003; length: P=0.412; N=9; Fig. 3D,E). Surprisingly, mitochondrial density was no different in processes when compared to the soma (P=0.721; Fig. 3F). This was unexpected as the nucleus excludes mitochondria, yet the volume of the nucleus is not excluded when calculating mitochondrial density in the soma. The implication is that, compared to the cytosol of cellular processes, mitochondrial density is considerably greater in the cytoplasmic shell that surrounds the nucleus in the soma.

Mitochondrial distribution shows signs of mutual exclusion

To determine whether mechanisms position mitochondria relative to each other, rather than simply disperse mitochondria throughout the length of neurons, we analyzed the distribution of distances between the centers of mitochondria (Fig. 4A-D; interneurons shown as an example group). We would expect a frequency distribution of distances to be described by an exponential decay if mitochondria are positioned randomly. The outcome of Kolmogorov–Smirnov (KS) tests of the cumulative distributions against exponentials enabled us to reject the likelihood that mitochondria are positioned randomly using a level of significance (α) of 0.05 (Fig. 4C). However, once α was corrected for the number of tests (α = 0.05/6 = 0.008; Bonferroni) we could not reject the likelihood that mitochondria are positioned randomly in most of the groupings of neurons (i.e. the distributions are mostly random; Fig. 4D).

The consistent departure from random when using an α of 0.05 might be ascribed primarily to a pattern observed in the frequency distributions in most neuron groupings, where mitochondrial spacings of ~1-5 μm are underrepresented (e.g. Fig. 4B-C). Interestingly, we observed that mitochondrial lengths formed a frequency distribution (Fig. 4E) that might fill the “void” in the distribution of mitochondrial spacings. Therefore, the void in Figure 4B might be attributed to an “occlusion effect”, where the center of one mitochondrion is displaced from the center of another mitochondrion by, on average, the length of a mitochondrion (the sum of two half lengths; 2.6 μm

for interneurons shown in Figures 4B and E). In fine neuronal processes such as these, mitochondria appear to have little opportunity to pass one another except at varicosities. This assessment receives some support from an analysis that shows that neuron diameters are not only greatest at the location of mitochondrial centers versus a random sampling of neuron diameters (Fig. 4F), but that neurons are even wider at locations where mitochondrial centers are no more than 1 μm apart, i.e. where they overlap. This analysis cannot determine causality, but the simplest explanation that fits the data without invoking molecular mechanisms to position mitochondria relative to one another, is that the distribution of mitochondria is the consequence of a physical limitation to mitochondrial passing except where opportunity is provided at varicosities.

Mitochondria are randomly distributed relative to pre- and post-synapses

To determine whether a mechanism positions mitochondria relative to pre- or post-synaptic specializations we analyzed the distribution of distances between each synapse and the center of the closest mitochondrion (Fig. 4G). KS tests of the cumulative distributions against exponentials are consistent with mitochondria being positioned independently of synapses (Fig. 4H-I). This result was consistent for both pre- and post-synaptic specializations in neurons grouped according to functional type or neurotransmitter type (Fig. 4J).

Synapses are not randomly distributed

Next, we turned our attention to the spacing between synapses (Fig. 5A-B). Our analysis rejected the likelihood that presynaptic specializations are positioned randomly in interneurons (Fig. 5C; interneurons shown as an example group). Our analysis also rejected the likelihood that post-synapses are positioned randomly (Fig. 5D), although the frequency distributions of distances between post-synaptic specializations are fundamentally different to those for pre-synapses. These results were largely consistent for synapses in neurons grouped according to functional type or neurotransmitter type (Fig. 5E). The clear discrepancy in glutamatergic sensory neurons is tentatively attributed to very low numbers (n=6).

Synapses localize to varicosities

In order to determine whether synapses localize to varicosities, we compared the diameter of neurons at sites of pre-synapses with the diameter at sites of post-synapses and with the average neuron diameter. In motor neurons and sensory neurons, pre-synapses, but not post-synapses, were found in the wider portions of the neurons (Fig. 5F). Whether synapse formation determines the site of varicosity formation, or varicosity formation determines the site of synapse formation is

not known, but co-localization of pre-synapses with varicosities has little impact on the resulting mitochondrial density at pre-synapses or post-synapses (Fig. 5G).

Mitochondria co-localize with varicosities rather than synapses

As mitochondria are most often found in varicosities (Fig. 4F), but pre-synapses also co-localize with varicosities (Fig. 5F), we tested the hypothesis that it is the synapses themselves, rather than varicosities, that are more influential in the placement of mitochondria. We did not test the possibility that mitochondria determine the distribution of varicosities (or synapses) as synapses and varicosities are stable on time scales over which mitochondria traverse long distances along these neuronal processes (add ref). We defined varicosities as swellings bounded by restrictions in neuronal diameter of at least 30% (Fig. 6A). We compared the proportion of synaptic varicosities bearing mitochondria to the proportion of non-synaptic varicosities bearing mitochondria (Fig. 6B). We found that these proportions were not statistically different in any neuron type, indicating that the presence of synapses did not predict a higher probability of an attendant mitochondrion (Fig. 6B). An analysis restricted to pre-synapses found within the pre-synapse rich mixed-synapse portion of GABAergic motor-neurons similarly yielded no indication of mitochondria localizing with synapses (P=0.491), indicating that such a phenomenon was not being missed because of averaging data from both pre- and post-synaptic compartments.

DISCUSSION:

For the purposes of Ca^{2+} buffering, the ready provision of ATP, or even the synthesis of neurotransmitters, a neuron might position mitochondria at synapses, yet we find little support for such control in the fine caliber neurons of *C. elegans*. In fact, our data are quite emphatic that these neurons do not systematically distribute mitochondria to synapses. To summarize, we could not dismiss the possibility that there is a random distribution of mitochondria relative to synapses (Fig.4G-J). Secondly, mitochondria are no more likely to be found in a varicosity with a synapse, than in a varicosity without a synapse (Fig. 6). Lastly, skirting the semantics of what does or does not constitute a varicosity, mitochondrial volume density is no greater at synapses than at any other location along thin processes (Fig. 5G). In the absence of evidence for the contention that the placement of mitochondria at synapses might be an advantageous design motif, we must reexamine our assumptions about what is advantageous for neuronal and neural function. It may be that neurons do not do this simply because it is not advantageous.

In this study, the average separation between synapses and their closest mitochondrion is approximately (Fig. 4G-J), raising the question of whether this separation is likely to impair function. The Ca^{2+} microdomains of voltage-gated Ca^{2+} channels extend no more than fractions of a micron (Naraghi and Neher, 1997), and mitochondria are generally well outside this range at most synapses. Therefore, considering the rapid rate at which Ca^{2+} equilibrates over distances in the range of 1-5 μm (Sala and Hernandez-Cruz, 1990), 5 μm may still be close enough to allow mitochondria to play a role in Ca^{2+} buffering in synaptic compartments, and for the Ca^{2+} to coordinate mitochondrial metabolism with synaptic activity (Chouhan et al., 2012). Similarly, a recent modelling approach predicted ATP levels to be remarkably stable in the cytosol between mitochondria, even when separated by tens of microns; albeit in the absence of inter-varicose restrictions (Kuznetsov and Kuznetsov, 2023). Lastly, while we know little about the presynaptic concentrations of GABA, acetylcholine and glutamate, and nothing about possible concentration gradients, synaptic vesicle reloading takes place at a far more measured pace than the events of Ca^{2+} triggered fusion (Nakakubo et al., 2020), in which case the loading mechanisms may have no need to draw on anything other than equilibrium concentrations of neurotransmitters.

Our observation of heterogeneity in mitochondrial morphometrics across neuron types (Fig. 2F-K) is consistent with previous findings in vertebrates and invertebrates (Shepherd and Harris, 1998; Cserep et al., 2018; Justs et al., 2022). Here, two findings deserve further discussion. First, we found that mitochondrial diameter is under exquisite control in the 190 to 250 nm range, to the extent that VC-type motor neurons have the capacity to deliver a diameter significantly different from the others, yet only ~20% less (Fig. 2H). The mechanisms controlling diameter are not known,

but simple restriction by the neuron itself does not appear to play a role as there is no correlation between mitochondrial diameter and neuronal diameter (Fig. S2B). Secondly, mitochondrial volume density falls into one of two ranges, likely reflecting different neuronal power demands. Four neuron types have a high mitochondrial volume density (5.7%, 6.2%, 6.7 and 7.1%), while one neuron type (VC-type MNs) is low (3.8%). The VC-type MN predominantly innervates the vulval muscles, which are only intermittently active, driving muscle contraction when eggs require expulsion (Collins et al., 2016). A comparison might be made with motor neurons in *Drosophila* larvae, where 3 motor neurons generate consistent motor patterns driving locomotion, with mitochondrial volume densities of 6.1%, 6.3% and 6.4%, while another motor neuron has a more phasic pattern of activity, and a low density of 3.9% (Justs et al., 2022).

Finally, while it is clear that the neurons examined here do not systematically distribute mitochondria to synapses, we might also consider the possibility that invertebrates such as *C. elegans* are either unable to do so, or do not gain an advantage by doing so. Certainly, *C. elegans* has orthologues of *miro* and *milton* (Mercer et al., 2009; Shen et al., 2016), although we know of no orthologue of syntaphilin (wormbase.org). Never-the-less, there is a staggering degree of conservation of cellular mechanisms between invertebrates and vertebrates, and so it seems likely that an organism with 20,000 protein-coding genes would have the capacity for subcellular control of mitochondria if it was to its advantage. Therefore, if vertebrates truly do distribute mitochondria to synapses, while *C. elegans* does not, it would seem most plausible that *C. elegans* simply does not gain an advantage from such a design motif. Clearly, *C. elegans* are different to vertebrates by virtue of their small size alone, operating at the “small-cell limit” (Lockery and Goodman, 2009). But two features in particular might diminish a need for mitochondria at synapses; their reliance on slow neuronal action-potentials rather than regenerative all-or-none action potentials (but see (Liu et al., 2018)), and a prominent role for Ca^{2+} influx in the absence of Na^{+} channels (Goodman et al., 1998). With slower and more sustained Ca^{2+} transients in synaptic compartments, mitochondrial placement would be less critical for the purposes of either Ca^{2+} buffering or for coordinating mitochondrial energy metabolism with neuronal energy metabolism.

MATERIALS AND METHODS

Electron Microscopy:

The electrons micrographs in *C. elegans*, examined in this manuscript, were prepared, fixed and reconstructed by White and others (White et al., 1986).

Measurement, Calibration and Analysis of Electron Micrographs:

Cross Sectional Area Measurements

3,607 slices from the N2U section (1844-ventral portion, 1763-dorsal portion) were analyzed with the Fiji ImageJ software. Each slice is 80 nm thick and 240 nm apart on average (White et al., 1986; Cook et al., 2019). Cross-sectional areas of neurons and mitochondria were measured using the freehand tool. Scales were cleared to zero for consistency of area measurements between researchers. To normalize area measurements between scanned micrographs we calibrated the areas of each micrograph according to measurements made between myosin filaments in muscle cross section. Using the straight-line selection tool, we twice sampled the length of 4 contiguous inter-myosin filament spacings, and averaged these two measurements. Cell body measurements, including those measurements on mitochondria within them, were separated from those made in the neuronal processes. Cell body measurements were those made in sections where the neuron diameter measurements of the processes exceeded 2 standard deviations of the diameter of the processes that led up to the cell body.

Calculation of Center-Center Distance Between Myosin Filaments

The separation between structures was calculated from an available image using Fiji and Matlab. The image was first processed in Fiji, utilizing the native “Thresholding” function with a range of 0-129. The results were modified with the Binary Erosion function until only the larger structures of interest remained. The “Particles” analysis was performed in order to obtain a list of all the structures and their positions in X and Y. Using Matlab, that list was then processed to calculate the distances between a point and every other point, for all points, utilizing a Euclidean distance calculation. The results were then filtered to consider only values larger than 0.04 microns and smaller than 0.06 microns. The statistics for the separation between adjacent points were thus calculated at a Mean of 0.048 microns separation, with a standard deviation of 0.005 microns.

Statistic	Value
Average	0.048241 µm
Standard Deviation	0.0048252 µm
Median	0.047822 µm
Variance	2.3283e-05 μm^2
N	*345*

Analysis

We calibrated the average myosin filament lengths using 48.3 nm from our center-to-center calculation.

Myosin filament Calibration Formula

$$193.2 * 193.2 \ / \ (average\ myosin\ filament\ length * average\ myosin\ filament\ length)$$

The neuronal and mitochondrial areas were multiplied by the calibrated myosin thick filament scale to normalize area measurements, from pixels to nanometers. Mitochondrial length was calculated by multiplying 240 nm (thickness of three micrographs) by the number of slices the mitochondria appears in. Mitochondrial volume was calculated by multiplying mitochondrial length by mitochondrial average area. Mitochondrial diameter was calculated by dividing mitochondrial average area by Pi, taking the square root and multiplying it by two. Instantaneous mitochondrial density was calculated by dividing mitochondrial average area by neuronal area. Neuronal volume was calculated by multiplying average neuronal area by neuronal length. Neuronal length was calculated by multiplying the sum of neuronal length by 240 nm (thickness of three sections). Average mitochondrial density was calculated by multiplying mitochondrial average volume by the number of mitochondria present in the neuron divided by neuronal volume.

Statistics:

Application of the discrete Kolmogorov-Smirnov (KS) model.

To test whether mitochondria are distributed randomly, we examine the distances between them. If mitochondria centers are distributed randomly along the axon and their locations are independent of each other, then the distance between consecutive mitochondria centers should follow an exponential distribution. Similarly, if synapses are distributed randomly and independently of each

other, then the distance between consecutive synapses should follow an exponential distribution. Finally, if mitochondria are distributed randomly and independently of synapses, then the distances between each synapse and the nearest mitochondrion should follow an exponential distribution.

To determine whether a distance distribution differs significantly from the exponential distribution, we used the bootstrap method and the KS statistic. First we fit the experimental distribution of distances using the maximum likelihood estimation. The resulting exponential parameter is simply the mean distance. Second, we computed the KS statistic for the experimental distribution by computing the maximum of the difference between the experimental and fitted cumulative distribution functions. Third, we drew 10,000 random samples from the fitted distribution, with the same sample size as the experimental sample. Fourth, we computed the KS statistic for each of those 10,000 bootstrap samples. To account for the fact that exponential parameter was not known in advance, each bootstrap sample is compared with the exponential distribution whose parameter matches its own mean distance. We also accounted for the fact that distances between mitochondria or synapse centers are always multiples of half the distance between EM section by rounding every value in the bootstrap samples to the nearest multiple of half the inter-section distance. Finally, we computed the fraction of bootstrap samples whose KS statistic was larger than the experimental sample's KS statistic, which is the P value. This analysis was performed using the Python programming language, including the KS test provided in the scipy module (scipy.stats.kstest).

Student's t-tests, ANOVA, and test for associations were performed in SigmaStat 3.5. Bonferroni's correction was used to adjust the level of α when multiple t-tests were applied. ANOVA was performed when multiple comparisons were applied and an overall α of <0.05 was required for significance. Pearson product-moment correlation coefficient was calculated to test the strength of associations.

Synapse Annotation:

Motor Neurons

DD3 – GABA: Ventral cord motor neurons, reciprocal inhibitors, change synaptic pattern during L1
VD5 – GABA: Ventral cord motor neuron, innervates vent body muscles, reciprocal inhibitor.
VD4 – GABA: Ventral cord motor neuron, innervates vent body muscles, reciprocal inhibitor.
VB4 – Cholinergic: Ventral cord motor neuron, innervates ventral body muscles.
VB5 – Cholinergic: Ventral cord motor neuron, innervates ventral body muscles.

VC1 – Cholinergic: Hermaphrodite specific ventral cord motor neuron innervates vulval muscles and ventral body muscles.
VC2 – Cholinergic: Hermaphrodite specific ventral cord motor neuron innervates vulval muscles and ventral body muscles.
VC3 – Cholinergic: Hermaphrodite specific ventral cord motor neuron innervates vulval muscles and ventral body muscles.

Interneurons – Cholinergic

AVAL- Ventral cord command interneuron
AVBL - Ventral cord command interneuron
AVAR- Ventral cord command interneuron
AVBR- Ventral cord command interneuron

Sensory Neurons – Glutamate

AVM- Anterior ventral microtubule cell, touch receptor
PVM- Posterior ventral microtubule cell, touch receptor

More information can be found on Wormatlas.org.

Blender Renderings:

Blender was used to render neurons in silhouette in Figures 1B and 3C. Using Blender's Python Application Programming Interface (API), calibrated radius, depth, and position data were imported into Blender (http://www.blender.org; RRID: SCR_008606). As a part of the python code, cylinders were populated with the radius and depth corresponding to each slice. The depth of each cylinder represents the distance between micrographs (240 nm) but these were adjusted in some instances to observe longer lengths of neuron (refer to scale bars in each figure). To represent any synapses present in each slice a set of different colored objects were created and assigned accordingly, where pink represents a post-synaptic terminal, blue represents a pre-synaptic terminal, and yellow represents both a pre-synaptic and post-synaptic terminal. The python code used to import the data, create the cylinders, and assign the corresponding materials can be found at: https://github.com/scrill2015/scrill2015/blob/de3fbc6afc4ec83d74fbdb8f48e322d71afc46a9/Modeling%20C.%20elegans%20Neurons%20in%20Blender%20with%20Python%20API

REFERENCES:

Chouhan AK, Ivannikov MV, Lu Z, Sugimori M, Llinas RR, Macleod GT (2012) Cytosolic calcium coordinates mitochondrial energy metabolism with presynaptic activity. J Neurosci 32:1233-1243.

Collins KM, Bode A, Fernandez RW, Tanis JE, Brewer JC, Creamer MS, Koelle MR (2016) Activity of the C. elegans egg-laying behavior circuit is controlled by competing activation and feedback inhibition. Elife 5.

Cook SJ, Jarrell TA, Brittin CA, Wang Y, Bloniarz AE, Yakovlev MA, Nguyen KCQ, Tang LT, Bayer EA, Duerr JS, Bülow HE, Hobert O, Hall DH, Emmons SW (2019) Whole-animal connectomes of both Caenorhabditis elegans sexes. Nature 571:63-71.

Cserep C, Posfai B, Schwarcz AD, Denes A (2018) Mitochondrial Ultrastructure Is Coupled to Synaptic Performance at Axonal Release Sites. eNeuro 5.

Devine MJ, Kittler JT (2018) Mitochondria at the neuronal presynapse in health and disease. Nat Rev Neurosci 19:63-80.

Goodman MB, Hall DH, Avery L, Lockery SR (1998) Active currents regulate sensitivity and dynamic range in C. elegans neurons. Neuron 20:763-772.

Hammond JW, Huang CF, Kaech S, Jacobson C, Banker G, Verhey KJ (2010) Posttranslational modifications of tubulin and the polarized transport of kinesin-1 in neurons. Mol Biol Cell 21:572-583.

Huang B, Jones SA, Brandenburg B, Zhuang X (2008) Whole-cell 3D STORM reveals interactions between cellular structures with nanometer-scale resolution. Nat Methods 5:1047-1052.

Justs KA, Lu Z, Chouhan AK, Borycz JA, Lu Z, Meinertzhagen IA, Macleod GT (2022) Presynaptic Mitochondrial Volume and Packing Density Scale with Presynaptic Power Demand. J Neurosci 42:954-967.

Kang JS, Tian JH, Pan PY, Zald P, Li C, Deng C, Sheng ZH (2008) Docking of axonal mitochondria by syntaphilin controls their mobility and affects short-term facilitation. Cell 132:137-148.

Kruppa AJ, Buss F (2021) Motor proteins at the mitochondria-cytoskeleton interface. J Cell Sci 134.

Kuznetsov IA, Kuznetsov AV (2023) ATP diffusional gradients are sufficient to maintain bioenergetic homeostasis in synaptic boutons lacking mitochondria. Int J Numer Method Biomed Eng 39:e3696.

Lebiedzinska M, Szabadkai G, Jones AW, Duszynski J, Wieckowski MR (2009) Interactions between the endoplasmic reticulum, mitochondria, plasma membrane and other subcellular organelles. Int J Biochem Cell Biol 41:1805-1816.

Liu Q, Kidd PB, Dobosiewicz M, Bargmann CI (2018) C. elegans AWA Olfactory Neurons Fire Calcium-Mediated All-or-None Action Potentials. Cell 175:57-70 e17.

Lockery SR, Goodman MB (2009) The quest for action potentials in C. elegans neurons hits a plateau. Nat Neurosci 12:377-378.

Mercer KB, Szlam SM, Manning E, Gernert KM, Walthall WW, Benian GM, Gutekunst CA (2009) A C. elegans homolog of huntingtin-associated protein 1 is expressed in chemosensory neurons and in a number of other somatic cell types. J Mol Neurosci 37:37-49.

Nakakubo Y, Abe S, Yoshida T, Takami C, Isa M, Wojcik SM, Brose N, Takamori S, Hori T (2020) Vesicular Glutamate Transporter Expression Ensures High-Fidelity Synaptic Transmission at the Calyx of Held Synapses. Cell Rep 32:108040.

Naraghi M, Neher E (1997) Linearized buffered Ca2+ diffusion in microdomains and its implications for calculation of [Ca2+] at the mouth of a calcium channel. J Neurosci 17:6961-6973.

Sala F, Hernandez-Cruz A (1990) Calcium diffusion modeling in a spherical neuron. Relevance of buffering properties. Biophys J 57:313-324.

Shen Y, Ng LF, Low NP, Hagen T, Gruber J, Inoue T (2016) C. elegans miro-1 Mutation Reduces the Amount of Mitochondria and Extends Life Span. PLoS One 11:e0153233.

Shepherd GM, Harris KM (1998) Three-dimensional structure and composition of CA3-->CA1 axons in rat hippocampal slices: implications for presynaptic connectivity and compartmentalization. J Neurosci 18:8300-8310.

Sigal YM, Speer CM, Babcock HP, Zhuang X (2015) Mapping Synaptic Input Fields of Neurons with Super-Resolution Imaging. Cell 163:493-505.

Turner NL et al. (2022) Reconstruction of neocortex: Organelles, compartments, cells, circuits, and activity. Cell 185:1082-1100 e1024.

Wang X, Schwarz TL (2009) The mechanism of Ca2+ -dependent regulation of kinesin-mediated mitochondrial motility. Cell 136:163-174.

White JG, Southgate E, Thomson JN, Brenner S (1986) The Structure of the Nervous-System of the Nematode Caenorhabditis-Elegans. Philosophical Transactions of the Royal Society B-Biological Sciences 314:1-340.

Winding M, Pedigo BD, Barnes CL, Patsolic HG, Park Y, Kazimiers T, Fushiki A, Andrade IV, Khandelwal A, Valdes-Aleman J, Li F, Randel N, Barsotti E, Correia A, Fetter RD,

Hartenstein V, Priebe CE, Vogelstein JT, Cardona A, Zlatic M (2023) The connectome of an insect brain. Science 379:eadd9330.

Figure 1

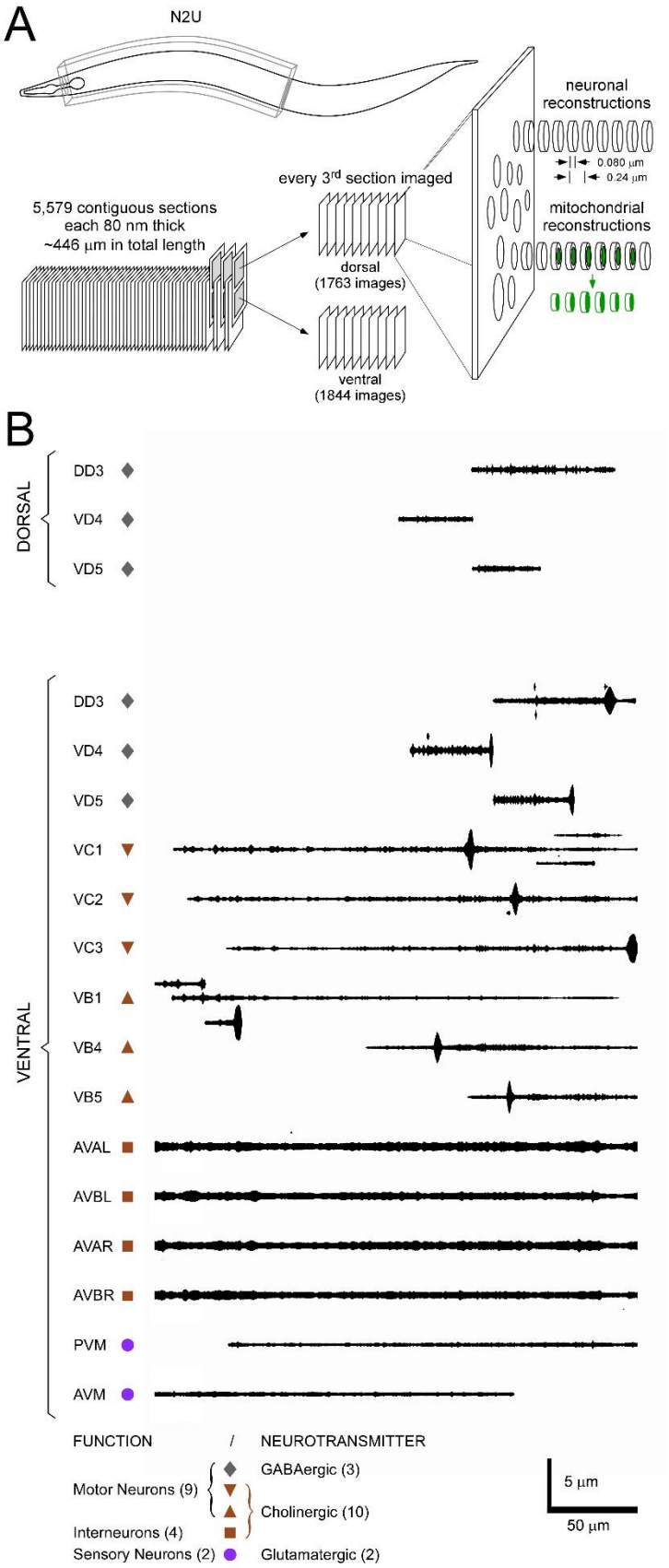
A
N2U
neuronal reconstructions
0.080 µm
0.24 µm
every 3rd section imaged
5,579 contiguous sections
each 80 nm thick
~446 µm in total length
mitochondrial reconstructions
dorsal
(1763 images)
ventral
(1844 images)
B
DORSAL
DD3
VD4
VD5
VENTRAL
DD3
VD4
VD5
VC1
VC2
VC3
VB1
VB4
VB5
AVAL
AVBL
AVAR
AVBR
PVM
AVM
FUNCTION / NEUROTRANSMITTER
Motor Neurons (9)
GABAergic (3)
Cholinergic (10)
Interneurons (4)
Sensory Neurons (2)
Glutamatergic (2)
5 µm
50 µm

Figure 2

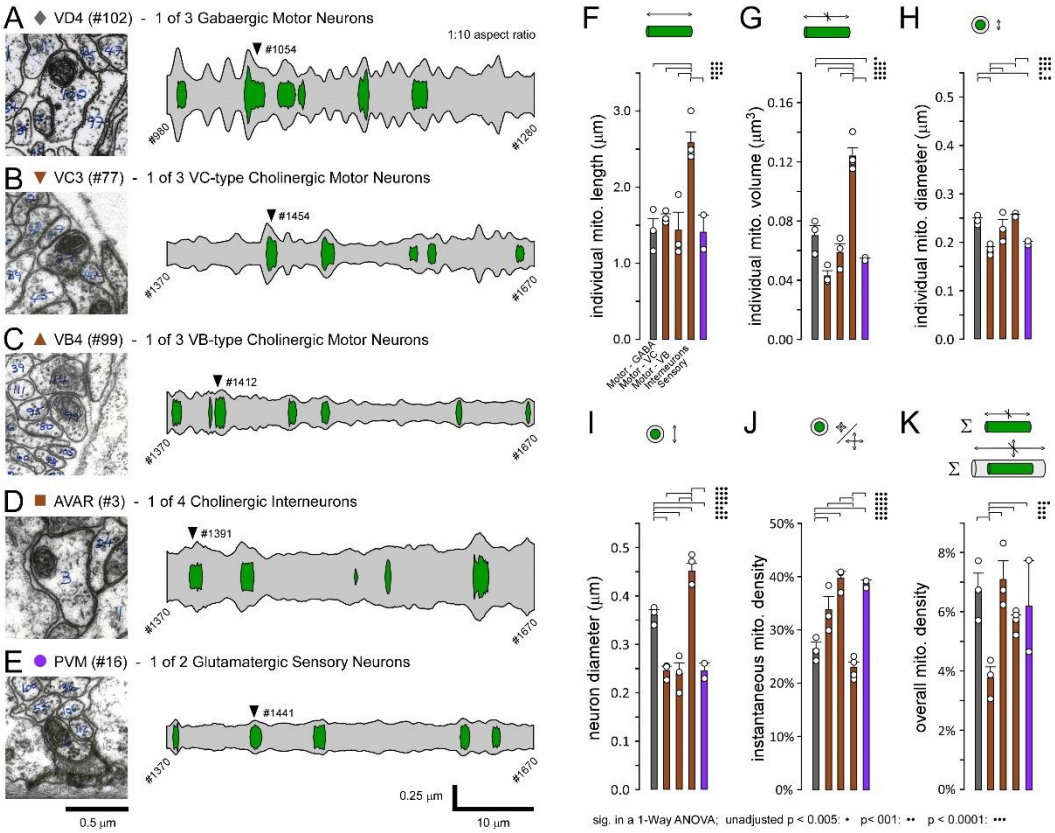
A VD4 (#102) - 1 of 3 Gabaergic Motor Neurons
1:10 aspect ratio
#1054
#980
#1280
B VC3 (#77) - 1 of 3 VC-type Cholinergic Motor Neurons
#1454
#1370
#1670
C VB4 (#99) - 1 of 3 VB-type Cholinergic Motor Neurons
#1412
#1370
#1670
D AVAR (#3) - 1 of 4 Cholinergic Interneurons
#1391
#1370
#1670
E PVM (#16) - 1 of 2 Glutamatergic Sensory Neurons
#1441
#1370
#1670
0.5 µm
0.25 µm
10 µm
F
G
H
I
J
K
individual mito. length (µm)
individual mito. volume (µm³)
individual mito. diameter (µm)
neuron diameter (µm)
instantaneous mito. density
overall mito. density
Motor - GABA
Motor - VC
Motor - VB
Interneurons
Sensory
sig. in a 1-Way ANOVA; unadjusted p < 0.005: • p< 001: •• p < 0.0001: •••

Figure 3

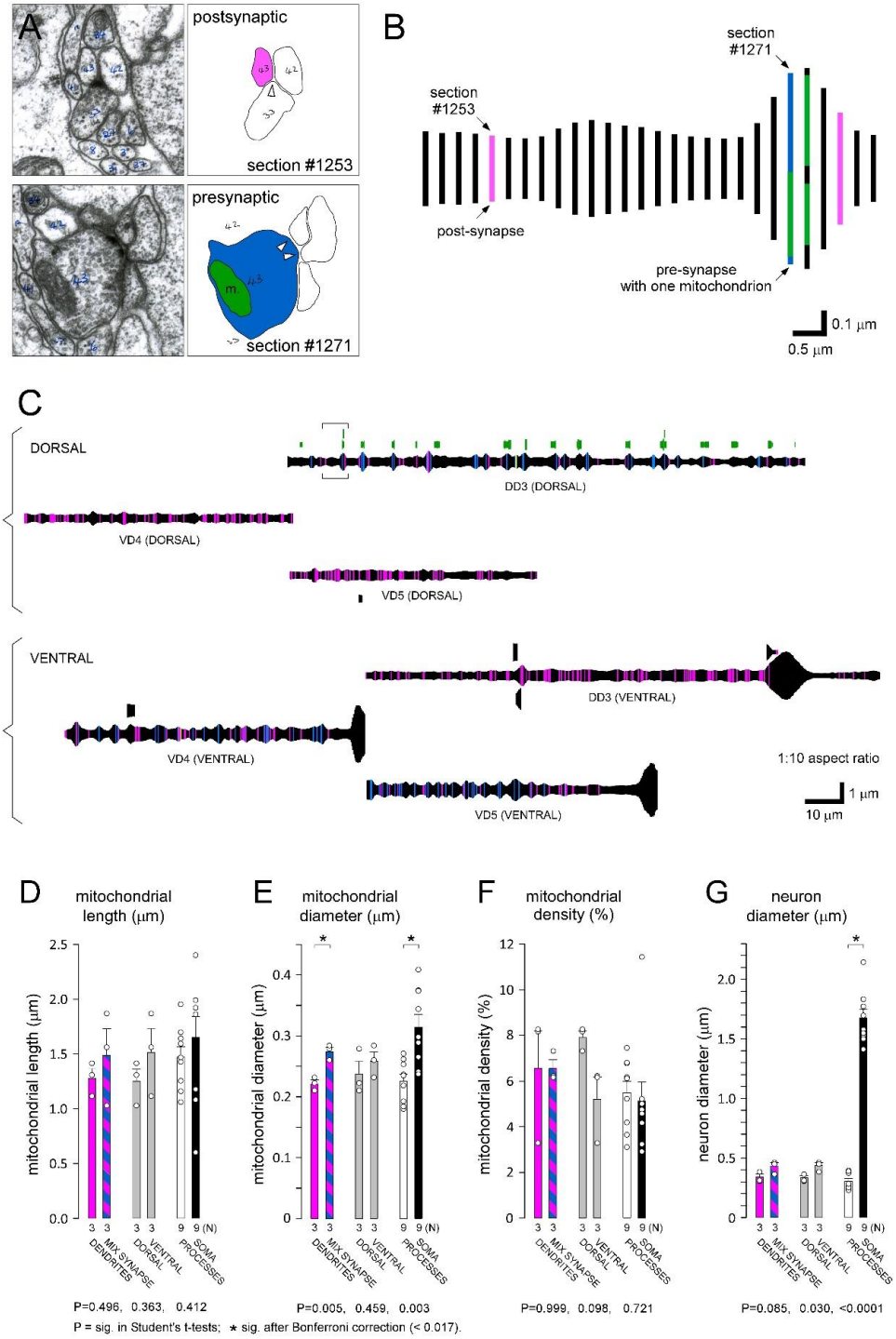
A
postsynaptic
section #1253
presynaptic
m.
section #1271
B
section #1253
section #1271
post-synapse
pre-synapse
with one mitochondrion
0.1 µm
0.5 µm
C
DORSAL
DD3 (DORSAL)
VD4 (DORSAL)
VD5 (DORSAL)
VENTRAL
DD3 (VENTRAL)
VD4 (VENTRAL)
VD5 (VENTRAL)
1:10 aspect ratio
1 µm
10 µm
D
mitochondrial length (µm)
mitochondrial length (µm)
E
mitochondrial diameter (µm)
mitochondrial diameter (µm)
F
mitochondrial density (%)
mitochondrial density (%)
G
neuron diameter (µm)
neuron diameter (µm)
3 3 3 3 9 9 (N)
MIX SYNAPSE DENDRITES
VENTRAL DORSAL
SOMA PROCESSES
P=0.496, 0.363, 0.412
P=0.005, 0.459, 0.003
P=0.999, 0.098, 0.721
P=0.085, 0.030, <0.0001
P = sig. in Student's t-tests; * sig. after Bonferroni correction (< 0.017).

Figure 4

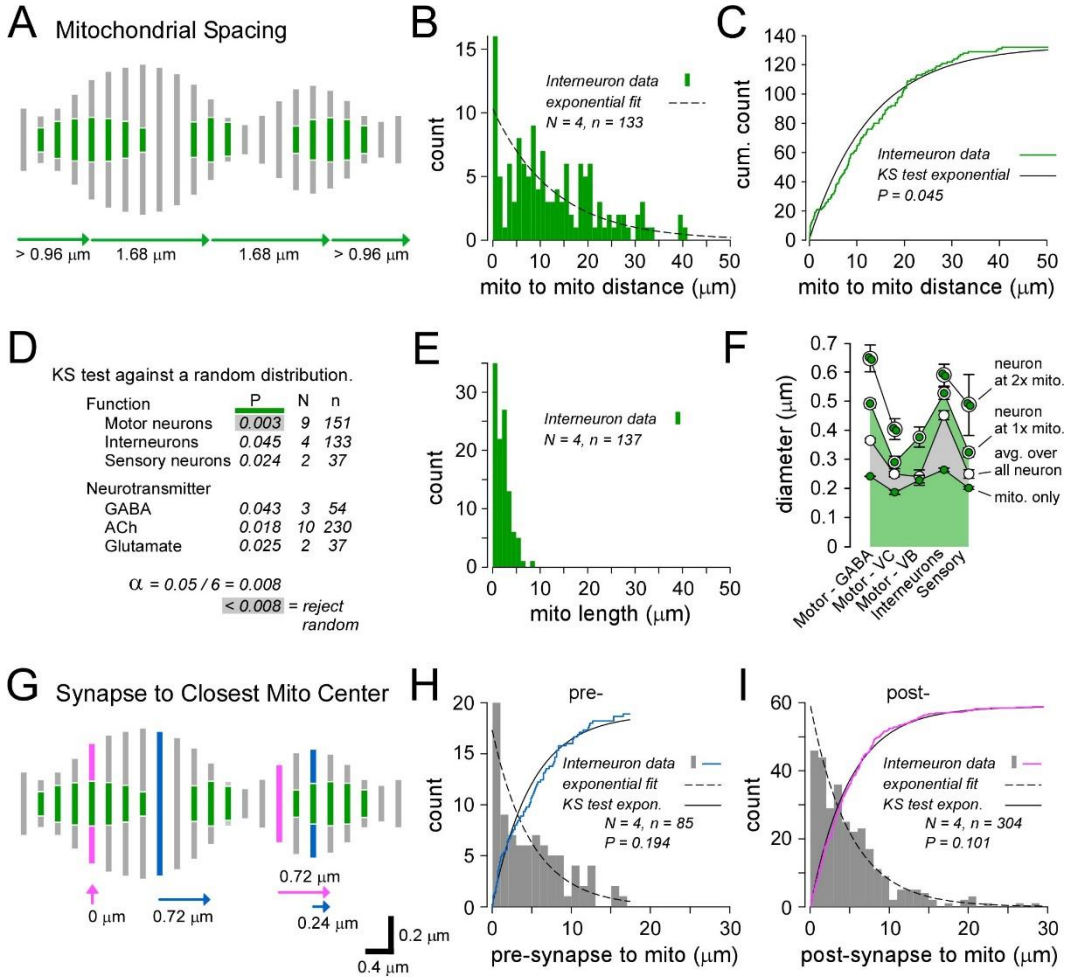
A
Mitochondrial Spacing
> 0.96 µm
1.68 µm
1.68 µm
> 0.96 µm
B
count
Interneuron data
exponential fit
N = 4, n = 133
mito to mito distance (µm)
C
cum. count
Interneuron data
KS test exponential
P = 0.045
mito to mito distance (µm)
D
KS test against a random distribution.
Function P N n
Motor neurons 0.003 9 151
Interneurons 0.045 4 133
Sensory neurons 0.024 2 37
Neurotransmitter
GABA 0.043 3 54
ACh 0.018 10 230
Glutamate 0.025 2 37
α = 0.05 / 6 = 0.008
< 0.008 = reject random
E
count
Interneuron data
N = 4, n = 137
mito length (µm)
F
diameter (µm)
neuron at 2x mito.
neuron at 1x mito.
avg. over all neuron
mito. only
Motor - GABA
Motor - VC
Motor - VB
Interneurons
Sensory
G
Synapse to Closest Mito Center
0 µm
0.72 µm
0.72 µm
0.24 µm
0.2 µm
0.4 µm
H
pre-
count
Interneuron data
exponential fit
KS test expon.
N = 4, n = 85
P = 0.194
pre-synapse to mito (µm)
I
post-
count
Interneuron data
exponential fit
KS test expon.
N = 4, n = 304
P = 0.101
post-synapse to mito (µm)
J
KS test against a random distribution.
Function P N n P N n
Motor neurons 0.276 9 212 0.304 9 292
Interneurons 0.194 4 85 0.101 4 304
Sensory neurons 0.070 2 20 - 2 3
Neurotransmitter
GABA 0.214 3 73 0.272 3 244
ACh 0.345 10 224 0.171 10 352
Glutamate 0.062 2 20 - 2 3
α = 0.05 / 6 = 0.008
< 0.008 = reject random

Figure 5

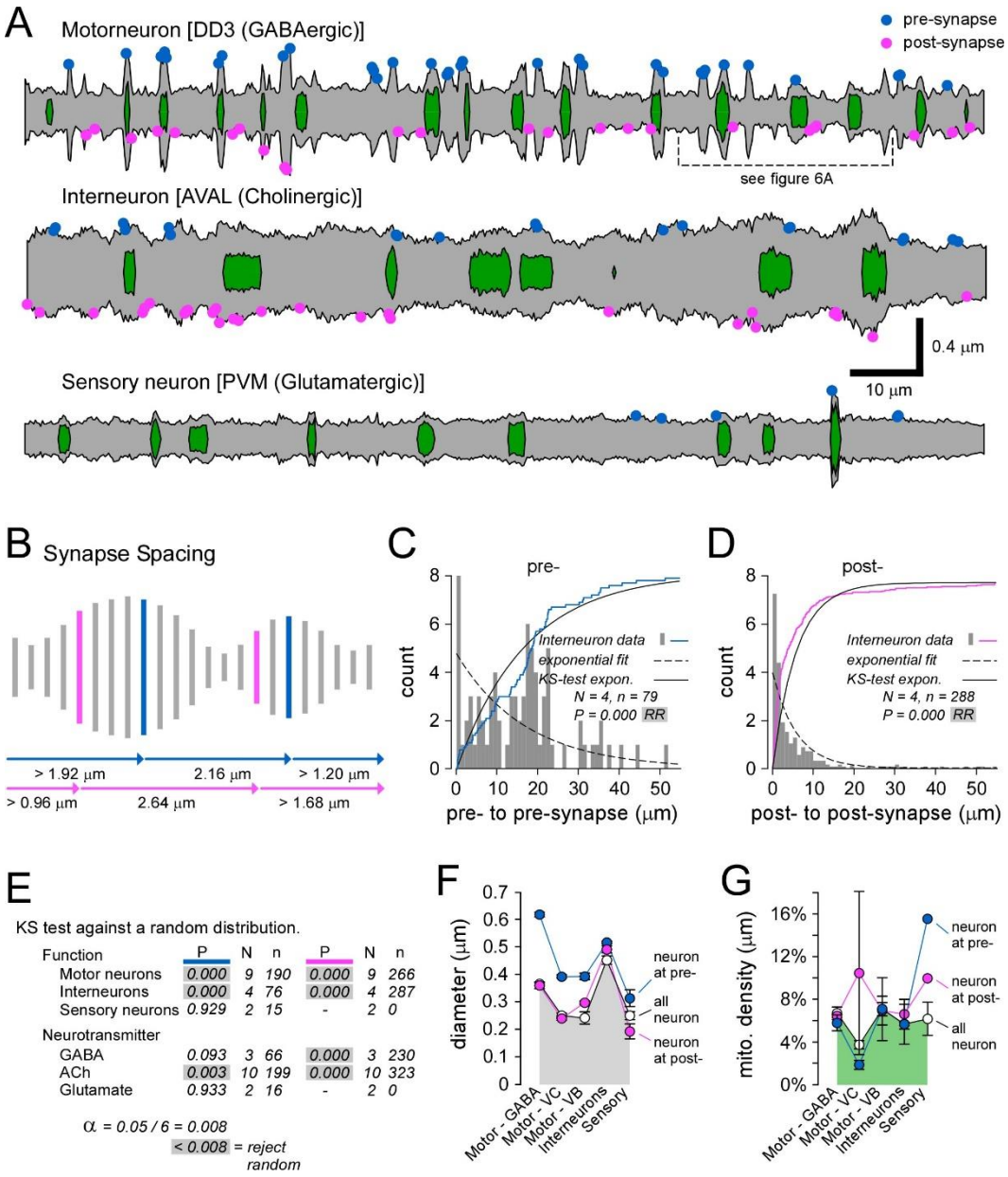
A
Motorneuron [DD3 (GABAergic)]
pre-synapse
post-synapse
see figure 6A
Interneuron [AVAL (Cholinergic)]
0.4 µm
10 µm
Sensory neuron [PVM (Glutamatergic)]
B Synapse Spacing
> 1.92 µm
2.16 µm
> 1.20 µm
> 0.96 µm
2.64 µm
> 1.68 µm
C
pre-
count
Interneuron data
exponential fit
KS-test expon.
N = 4, n = 79
P = 0.000 RR
pre- to pre-synapse (µm)
D
post-
count
Interneuron data
exponential fit
KS-test expon.
N = 4, n = 288
P = 0.000 RR
post- to post-synapse (µm)
E
KS test against a random distribution.
Function P N n P N n
Motor neurons 0.000 9 190 0.000 9 266
Interneurons 0.000 4 76 0.000 4 287
Sensory neurons 0.929 2 15 - 2 0
Neurotransmitter
GABA 0.093 3 66 0.000 3 230
ACh 0.003 10 199 0.000 10 323
Glutamate 0.933 2 16 - 2 0
α = 0.05 / 6 = 0.008
< 0.008 = reject random
F
diameter (µm)
neuron at pre-
all neuron
neuron at post-
Motor - GABA
Motor - VC
Motor - VB
Interneurons
Sensory
G
mito. density (µm)
neuron at pre-
neuron at post-
all neuron
Motor - GABA
Motor - VC
Motor - VB
Interneurons
Sensory

Figure 6

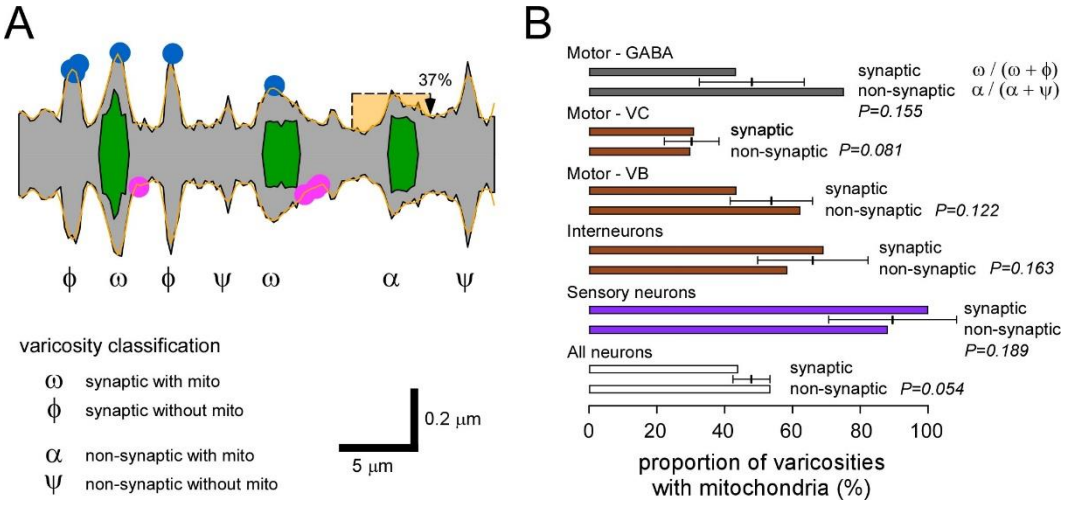
A
37%
ϕ ω ϕ ψ ω α ψ
varicosity classification
ω synaptic with mito
ϕ synaptic without mito
α non-synaptic with mito
ψ non-synaptic without mito
0.2 μm
5 μm
B
Motor - GABA
synaptic
non-synaptic
ω / (ω + ϕ)
α / (α + ψ)
P=0.155
Motor - VC
synaptic
non-synaptic P=0.081
Motor - VB
synaptic
non-synaptic P=0.122
Interneurons
synaptic
non-synaptic P=0.163
Sensory neurons
synaptic
non-synaptic
P=0.189
All neurons
synaptic
non-synaptic P=0.054
0 20 40 60 80 100
proportion of varicosities
with mitochondria (%)

Figure S1

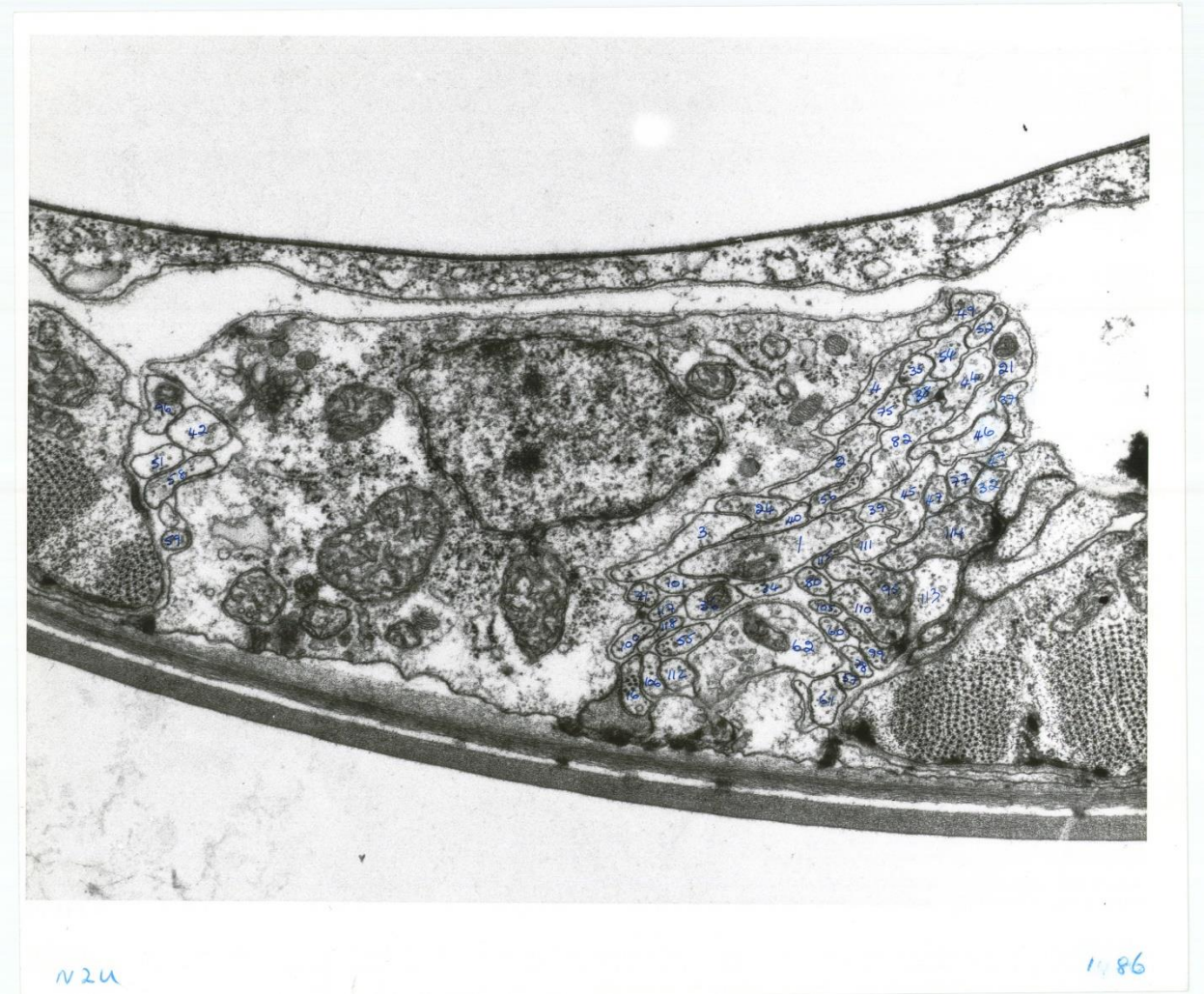

Figure S2

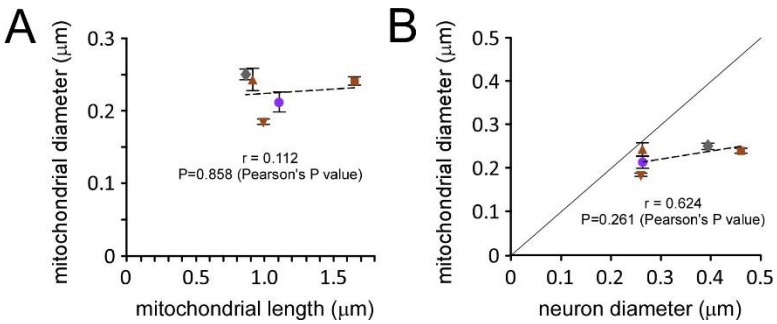

LEGENDS

Figure 1. 3D reconstruction of 15 neurons from an electron micrograph series through a worm.

(A). Schematic of the N2U series in *C elegans* and the workflow from contiguous micrographs to reconstructions using neuronal and mitochondrial cross-sectional areas measured in ImageJ. The series spans the anterior portion of a hermaphroditic worm and is composed of 5579 sections, each 80 nm thick. Photomicrographs were taken of every 3rd section covering a portion between the posterior extent of the nerve ring and the vulva. We analyzed 1844 contiguous micrographs on the ventral side, posterior to the nerve ring and neuropile. 1763 contiguous micrographs were analyzed on the dorsal side. Each area measurement represents the average for a section, separated from the next by 160 nm (240 nm in total).

(B). Silhouette reconstructions of 15 neurons. A legend for the symbols beside individual neuron names is shown at the bottom. Individual GABAergic motor neurons (DD3, VD4, VD5) have a dorsal and a ventral extent. Enlarged swellings indicate cell bodies captured in this micrograph series for some of the neurons (DD3, VD4, VD5, VC1, VC2, VC3, VB1, VB4, VB5). Branches are represented on one (VD4, VC2) or both (DD3, VC1, VB1) sides of the primary axis of some neurons. Anterior to posterior: left to right. Name acronyms: Dorsal D-type Motor Neuron 3 (DD3); Ventral D-type Motor Neurons 4 and 5 (VD4 and VD5); Ventral B-type Motor Neurons 1, 4 and 5 (VB1, VB4 and VB5); Ventral C-type Motor Neuron 1, 2 and 3 (VC1, VC2 and VC3); Anterior Ventral Processes A Left and Right (AVAL and AVAR); Anterior Ventral Processes B Left and Right (AVBL and AVBR).

Figure 2. Mitochondrial morphometrics differ according to neuronal function.

A-E. 2D reconstructions of example neurons from different 5 classes, along with their mitochondria. Left panels: 1 μm x 1 μm regions of interest cropped from single micrographs in the N2U series. Right panels: neurons and mitochondria reconstructed from area measurements made in each of 301 micrographs. Profiles smoothed with a 5-point moving average. Neuron identity and neurotransmitter type indicated above each micrograph in A-E. Arrowheads show the number and location of each example micrograph.

F-K. Plots comparing mitochondrial and neuronal morphometrics between 15 neurons divided into their functional and neurotransmitter type.

F. For each neuron, individual mitochondrial length was calculated by multiplying the number of slices by 0.24 μm.

G. Individual mitochondrial volume was calculated by multiplying the average mitochondrial area by the length of the mitochondrion.
H. Individual mitochondria diameter was calculated by dividing the average mitochondria area by pi, then taking the square root and multiplying by 2.
I. Neuronal diameter was calculated by dividing the average neuronal profile area by pi, then taking the square root and multiplying by 2.
J. Instantaneous mitochondrial density was calculated by dividing summed mitochondrial areas by the neuronal profile area (the latter including both cytosolic and mitochondrial areas) across all micrographs where the neuron contained a mitochondrion.
K. Overall mitochondrial density was calculated by dividing summed mitochondrial areas by summed neuronal profile areas.
Areas were calibrated according to the number of pixels that spanned the known distance between thick filaments in the cross-sectioned muscle. See methods and materials for further details.
One-way ANOVAs show significance at four levels: 0.005 (1 dot), 0.001 (2 dots), 0.0001 (3 dots). $\alpha = 0.005$ represents an $\alpha = 0.05$ Bonferroni correction across 10 tests.

Figure 3. Mitochondrial morphometrics show few differences across subcellular compartments in motor neurons.
A. Upper image: micrograph of section 1253 where GABAergic motor neuron DD3 is post synaptic to ventral cord motor neuron DB3. Lower image: micrograph of section 1271 where GABAergic motor neuron DD3 is presynaptic to dBWMR11 (body wall muscle); mitochondria indicated in green.
B. Schematic of dorsal portion of GABAergic motor neuron DD3 from 1249-1276. Locations of pre and post synapse micrographs illustrated in A. Mitochondria indicated in green.
C. Reconstructions of 3 different GABAergic motor neurons; DD3, VD4, VD5. Postsynapse indicated in pink, presynapses indicated in blue, mitochondria indicated in green. Large swellings indicate cell bodies and short processes near the main neuron indicate branches.
D. E. F. G. Plots comparing mitochondria length, diameter, density and neuron diameter within dendrites, mixed portions of the cell, and soma. Calculations for length, diameter, density are the same as in figure 2. Student t-test with Bonferroni alpha level correction for 3 tests ($\alpha = 0.05 / 3 = 0.017$).

Figure 4. Analyses of mitochondrial positioning along fine neuronal processes.
A. Schematic of a sectioned neuron with mitochondria. Distances from the center of one mitochondrion to the next mitochondrion, anterior-to-posterior, indicated with arrows.
B. Frequency distributions of distances between mitochondria in cholinergic interneurons.

C. A cumulative plot is shown, along with a Kolmogorov–Smirnov (KS) test against an exponential (P=0.045). The Bonferroni alpha level correction for 6 tests (panel D) is 0.008 (α = 0.05 / 6) so we are unable to reject the null that the samples are drawn from a random distribution of spacings.
D. The results of KS tests against random distributions.
E. A Frequency distribution of the length of mitochondria in the same cholinergic interneurons analyzed in panels B and C.
F. Average diameters of mitochondria, neurons, neurons at the location of single mitochondria, and neurons at the location of overlapping mitochondria. Cell bodies were excluded. Two-way ANOVA performed on mean neuronal diameters. Neurons had a significantly greater diameter at presynapses, but not at postsynapses. Neurons had a significantly greater diameter when a mitochondrion was present, and an even greater diameter when two were present (overlapping). Neuron type factor: $p<0.001$, $F(4,13)=27.4$; mitochondria number present factor (0, 1 and 2): $p<0.001$, $F(2,13)=49.5$.
G. Schematic of a sectioned neuron with AZs and mitochondria, showing the spacings that were analyzed. Pre-synapses indicated in blue, post-synapses indicated in pink and mitochondria in green. Distances from each AZ to the closest mitochondrion center are indicated with arrows.
H-I. Frequency distributions of distances to mitochondria, measured from cholinergic interneuron pre- (H) and post-synapses (I). Cumulative plots are shown for each, along with KS tests against exponentials (P = 0.194 and P=0.101; in both cases unable to reject the null that the samples are drawn from a random distribution of spacings).
J. The results of KS tests against random distributions.

Figure 5. Analyses of synapse positioning along fine neuronal processes.
A. Neuronal plasma membrane, mitochondria and synaptic locations, reconstructed from measurements made in each of 551 contiguous micrographs (#1213 to #1763; 132 μm; without profile smoothing).
B. Schematic of a sectioned neuron showing the distances from one pre-synapse to the next pre-synapse (blue arrows), and from one post-synapse to the next post-synapse (pink arrows).
C-D. Frequency distributions of distances from one synapse in a cholinergic interneuron to the next; pre- (C) and post-synapses (D). Cumulative plots are shown for each, along with KS tests against exponentials (P = 0.000 and 0.000), allowing us to reject the null that the samples are drawn from a random distribution.
E. The results of Kolmogorov–Smirnov (KS) tests against random distributions.
F. Average diameters of neurons, neurons at the location of a pre-synapse (blue), and at the location of post-synapses (pink). Two-way ANOVA performed on mean neuronal diameters.

Neurons had a significantly greater diameter at presynapses, but not at postsynapses. Neuron type factor: $p<0.002$, $F(1,4)=12.3$; compartment identity factor (all, pre or post): $p<0.004$, $F(2,2)=11.6$.
G. Average mitochondrial density at the location of a pre-synapse (blue), and at the location of post-synapses (pink). Two way ANOVA performed on mean mitochondrial density. There was no significant difference in mitochondrial density at presynapses or postsynapses. Neuron type factor: $p=0.908$, $F(4,12)=0.236$; compartment identity factor (all, pre or post): $p=0.313$, $F(2,12)=1.420$.

Figure 6. A varicosity is not more likely to contain a mitochondrion if it contains a synapse.
A. The profile of a motor neuron (dorsal aspect of DD3), its mitochondria and synaptic locations, reconstructed from measurements made in each of 126 contiguous micrographs (#1588 to #1713; 30 μm) before (black trace) and after (orange trace) smoothing with a 3-point moving average. A 5 micron "hat" was placed on each swelling, and defined as a varicosity if bounded on both sides by a restricted diameter at least 30% less that the diameter of the swelling. The hat could be placed off-center, but the restrictions needed to be found with the length of the hat. Seven swellings were defined as varicosities; 4 with synapses ($\omega + \phi$), and 3 without ($\alpha + \psi$). The proportion of synaptic varicosities bearing mitochondria can be calculated as [$\omega/(\omega + \phi)$ = 2/4 = 50%], while the proportion of non-synaptic varicosities bearing mitochondria can be calculated as [$\alpha / (\alpha + \psi)$ = 1/3 = 33%].
B. A comparison of the proportion of synaptic varicosities bearing mitochondria to the proportion of non-synaptic varicosities bearing mitochondria, across neurons of different functional type. Z-tests for differences between proportions found no significant differences within any neuron type. The average pooled proportion is indicated, along with error bars.

Supplemental Figure 1:
Example micrograph (N2U series #1486) from the ventral side of the worm.

Supplemental Figure 2:
A. The regression of mitochondrial diameter on neuron diameter showed no correlation ($r=0.622$, $p=0.261$), which would be expected if neuronal diameter is not a key determinant of mitochondrial diameter.
B. The regression of mitochondrial diameter on mitochondrial length also showed no correlation ($r=0.122$, $p=0.858$).
Pearson's correlation coefficients were calculated in both cases. Data and statistics reported in Extended Data Tables.